

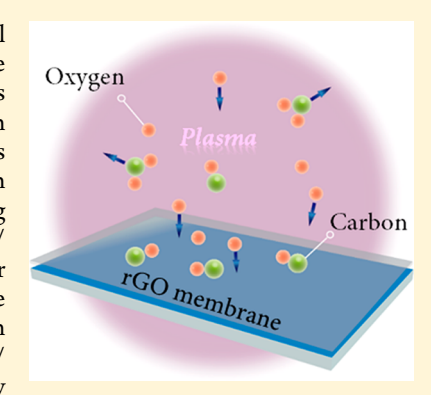
# Tuning Water Nanofiltration Performance of Few-Layered, Reduced Graphene Oxide Membranes by Oxygen Plasma

Weiwei L. Xu, Fanglei Zhou, and Miao Yu\*®

Department of Chemical and Biological Engineering, Rensselaer Polytechnic Institute, Troy, New York 12180, United States

Supporting Information

ABSTRACT: Ultrathin, graphene oxide (GO) membranes have shown great potential for water nanofiltration applications. However, due to the difficulties in controlling the intrinsic oxygen-containing functional groups on GO and the swelling of GO interlayers in aqueous solution, it is highly challenging to tune GO membranes' nanofiltration performance by adjusting their hydrophilicity and interlayer nanochannel size. In this study, oxygen plasma was reported as an effective technique to tune water nanofiltration performance of few-layered, reduced graphene oxide (rGO) membranes, by improving rGO membranes' hydrophilicity and/or adjusting effective permeation nanochannel/ pore sizes. The 5 nm thick GO membranes were fabricated through a layer-by-layer deposition method and subsequently reduced at 220 °C under vacuum. No detectable water permeance (<1.0 L/(m²·h·bar)) under 5 bar pressure drop suggests the high quality of the rGO membranes possibly with very small hydrophobic nanochannels/ pores. Exposure to oxygen plasma for different time intervals (0-30 s) gradually improved the hydrophilicity of the rGO membranes, with the water contact angle



decreasing from 74 to 31°. This is consistent with X-ray photoelectron microscopy results showing gradual increase of oxygencontaining functional groups with the increase of oxygen plasma etching time. By tuning membrane properties upon different oxygen plasma exposure times, the 5 nm thick rGO membranes showed the optimum nanofiltration performance with water permeance of 44 L/( $m^2$ ·h·bar) and 98% rejection for methylene blue. Oxygen plasma treatment, therefore, may provide a viable way for tuning few-layered, graphene-based membranes for highly efficient water nanofiltration applications.

## 1.0. INTRODUCTION

Rapid industrialization and urbanization has made the shortage of clean water a worldwide issue. High demand for clean water has motivated us to develop highly efficient, costeffective, and environmentally friendly water treatment technologies.<sup>2,3</sup> Compared with other water purification methods, such as distillation, chemical precipitation and adsorption etc., 4,5 membrane-based water treatment technologies are not only more economic but also being commercially demonstrated having high efficiency in removing salts and contaminants from water. 6-9

Emerging as new promising membrane materials, graphene and its derivatives have attracted great attention; their favorable two-dimensional structure, atomically thin thickness, high chemical stability, 10 and strong mechanical strength, allow the fabrication of ultrathin membranes with high quality for high flux separations. 12-17 Previous computational studies suggested that the single-layered graphene with subnanometer pores may provide greatly improved permeability and selectivity for water separation, 18-21 and potential of applying single-layered nanoporous graphene in desalination and selective ionic transport was further demonstrated by recent laboratory work.<sup>22–26</sup> Although ionic bombardment,<sup>24</sup> e-beam lithography,<sup>27</sup> plasma<sup>26,28</sup> and UV-induced etching<sup>29</sup> have been attempted to generate selective pores on graphene, for practical applications it is still very challenging to precisely

control the generating of pores on single-layered graphene membranes by using these techniques. Besides, reliable and scalable techniques for fabricating defect-free, single-layered graphene-based membranes as an ideal substrate for etching are still missing. Compared with single-layered graphene, fewlayered reduced graphene oxide (rGO) membranes could not only be prepared by practical solution-based deposition process and subsequent reduction but also work as reliable bases or platforms allowing better control over the surface etching process.

Our previous work showed that rGO membranes, prepared by removing significant amount of oxygen-containing functional groups via appropriate reduction, had an interlayer nanochannel size of approximately 0.43 to 0.62 nm, as suggested by the good ideal selectivity of hexane (kinetic diameter: 0.43 nm) over 2,2-dimethylbutane (kinetic diameter:  $0.62 \, \text{nm}).^{30}$  In comparison with GO membranes, rGO membranes have much narrower and probably much more hydrophobic nanochannels that are good candidates for further size and hydrophilicity tuning, if a desired technique can be

Special Issue: Richard Noble Festschrift

Received: May 18, 2018 Revised: June 21, 2018 Accepted: June 26, 2018 Published: June 26, 2018

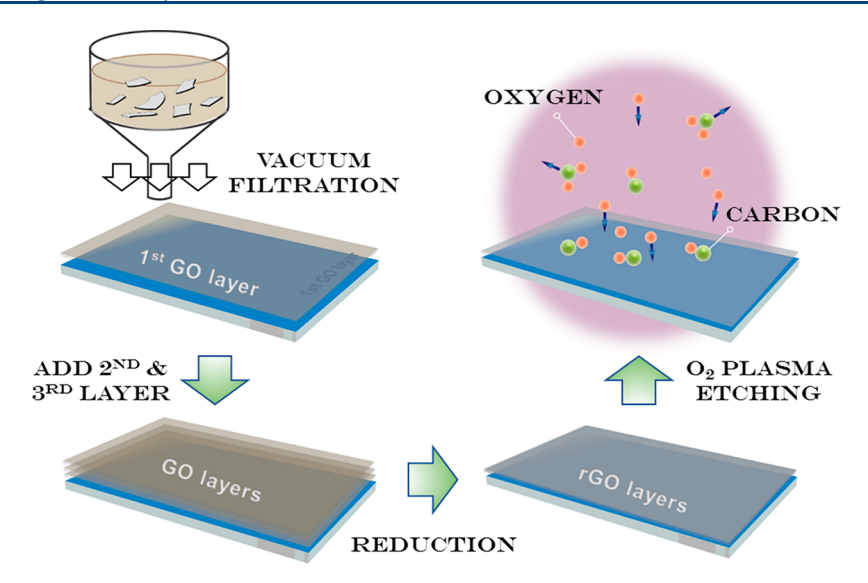


Figure 1. Schematic illustration of layer-by-layer deposition to prepare GO membrane, thermal reduction of GO membrane in the vacuum to obtain a tight layered structure, and etching with oxygen plasma treatment to tune hydrophilicity and effective pore/nanochannel size.

identified, to achieve highly efficient water nanofiltration. 31–34 Plasma treatment has been proved as an effective technique for both modifying surface property and creating pores with suitable size on rGO membranes, and as a result significantly improved their water permeability. 35,26,28 In this study, we explored the potential of using oxygen plasma for tuning hydrophilicity and effective transport nanochannel/pore size of few-layered rGO membranes, and investigated water nanofiltration performance of oxygen plasma treated rGO membranes.

The procedure for preparing oxygen plasma treated rGO membranes is schematically shown in Figure 1. First, fewlayered rGO membranes with high quality were prepared by depositing large, single-layered GO (SLGO) flakes through a simple layer-by-layer deposition process (see details in Experimental Section) and followed by thermal reduction at 220 °C for 12 h in a vacuum; then, rGO membranes were treated under oxygen plasma for different times (0-30 s) to reoxidize and etch pores on rGO. The SLGO flakes and asprepared rGO membranes before and after oxygen plasma treatment were characterized by atomic force microscopy (AFM), scanning electron microscopy (SEM), X-ray photoelectron spectroscopy (XPS), Raman, Fourier transform infrared (FTIR) and X-ray diffraction (XRD); pure water permeation and dye removal ability of oxygen plasma treated rGO membranes were measured to understand influence of oxygen plasma on water nanofiltration performance.

## 2.0. EXPERIMENTAL SECTION

**Material and Chemicals.** All the chemicals, including NaNO<sub>3</sub>, methylene blue (MB), concentrated sulfuric acid (H<sub>2</sub>SO<sub>4</sub>, 99.99%), potassium permanganate (KMnO<sub>4</sub>), hydrochloric acid (HCl, 37%), and hydrogen peroxide (H<sub>2</sub>O<sub>2</sub>, 30% (w/w)) were purchased from Sigma-Aldrich and used without further purification. Expandable graphite (Grade 1721-Asbury Carbon) was supplied by Asbury Carbon for GO synthesis.

**Membrane Fabrication.** The GO membranes were deposited on a commercially available anodized aluminum oxide (AAO) substrate (GE Healthcare) through a layer-by-layer (LBL) vacuum filtration process. To cover the AAO substrate (effective area: 10.5 cm<sup>2</sup>) with a monolayer of GO,

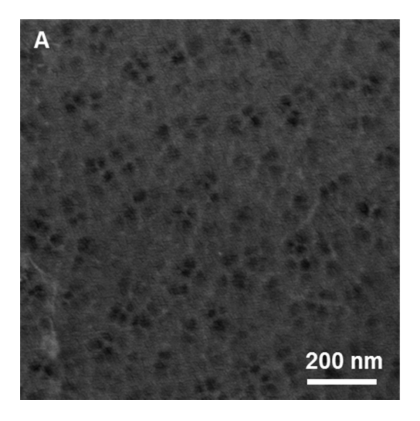
theoretically 1.07  $\mu g$  of SLGO is needed. The first layer of GO was deposited by filtering 250 mL of GO dispersion with concentration of 4.3  $\times$  10<sup>-6</sup> mg/mL through an AAO substrate; it took about 15 min to complete the whole filtration process, and the next layer of GO was deposited after the previous layer was completely dry. Finally, GO membranes were reduced in a vacuum at 220 °C for 12 h. The ultrathin rGO membranes reported in this work were prepared through three times of LBL deposition.

Oxygen plasma (UNITRONICS PE-50) treatments were applied on the surface of the rGO membranes. Etching treatments were performed under vacuum of 200 mTorr with power supply of 400 W 50 kHz, the oxygen flow was fixed to 25 cc/min, the distance between rGO membrane and plasma source was ~10 cm, and different etching time intervals were applied to study the influence of etching time on the nanofiltration performance of rGO membranes.

Membrane Permeation Test. Pure water permeance and dye rejection of plasma etched rGO membranes were measured in a dead-end system purchased from Sterlitech Inc. and driven by N<sub>2</sub> gas under a pressure drop of 5 bar. The permeation area was 19.6 mm<sup>2</sup>, and the chosen sample was fixed at the bottom of the water tank. The water permeance was obtained by measuring the weight of DI water collected with permeation time for at least 48 h. Steady state water flux was reported after permeation reached steady state for at least 2 h. Rejection for MB was measured to evaluate nanofiltration performance of plasma etched rGO membranes; MB concentration of the feed solution was 6.4 mg/L, and 50 mL feed solution was added into the dead-end system and stirred at 500 rpm. After 2 h of equilibrium, the concentration of MB in 3 mL collected permeate was analyzed using UV-vis spectrophotometer (Shimadzu UV-1800). The rejection (R) of MB was calculated by  $R = 1 - \frac{C_p}{C_f}$ , where  $C_p$  and  $C_f$  are the MB concentration in permeate and feed, respectively.

#### 3.0. RESULTS AND DISCUSSION

Graphene oxide used in this work was synthesized by Hummers method.<sup>36</sup> The large size, SLGO flakes were exfoliated by the freeze–thaw technique (see details in



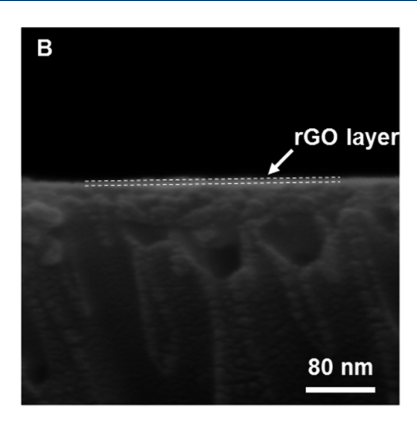


Figure 2. FESEM images of the triple-layered rGO membrane: (A) surface and (B) cross section.

Supporting Information).<sup>37</sup> AFM image, shown in Figure S1A, confirms the single layer feature of the GO flakes with a lateral size of  $1-2 \mu m$ . The Raman spectrum (Figure S1B) shows a G peak at ~1590 cm<sup>-1</sup> and a D peak at ~1350 cm<sup>-1</sup>, confirming the sp<sup>2</sup> hybridization of graphic carbon and distortion of carbon lattice. 38,39 The as-prepared SLGO flakes exhibit characteristic FTIR peaks (Figure S1C) of -C=O stretching at 1760 cm<sup>-1</sup>, C-O-C stretching at 1220 cm<sup>-1</sup>, and -OH stretching at 3500 cm<sup>-1</sup>, which correspond well to the GO structure typically reported and indicate the presence of unoxidized graphic carbon and various oxygen-containing groups on the GO flakes. The XPS spectra (Figure S1D) show that about 49% of carbon is not oxidized, 41% bonded in C-O, and 10% bonded in C=O and COOH.

When SLGO flakes stack on top of each other and form a lamellar structure, the oxygen-containing functional groups, such as hydroxyl, epoxy and carbonyl groups, act as spacers to keep distance of adjacent SLGO flakes. Because of the strong hydrophilicity of these functional groups, water can easily intercalate into GO layer and cause swelling of GO membranes, which not only decreases the membrane selectivity of water over salts or small organic molecules but also reduces the membrane stability. 40,41 To explore the possible structure difference between GO and rGO membranes under dry and wet conditions, XRD was performed to measure average interlayer spacing (d-spacing); XRD measurements were conducted on thick GO and rGO membranes (1-2  $\mu$ m) to obtain better signals. Figure S2A shows the XRD pattern of dry GO membrane with a characteristic peak located at 11.06°, corresponding to a d-spacing of 7.8 Å; after soaking dry GO membrane in DI water for 24 h, the peak shifted to 10.4°, indicating the expansion of d-spacing to 8.9 Å. Reduction of GO membranes may help "locking" the interlayer d-spacing and thus increase the membrane stability in water. Upon reduction, the characteristic peak of the rGO membrane moved to 23.9° (Figure S2B), corresponding to a d-spacing of 3.7 Å; after soaking it in water for 24 h, no peak shift was observed, suggesting the interlayer spacing was locked and could not expand in water. Therefore, considering the longterm stability of rGO membranes in water and their narrower hydrophobic interlayer channels (4.3–6.2 Å), 30 they may serve as ideal platforms/starting membranes that can be transformed into high performance water nanofiltration membranes by tuning nanochannel size and hydrophilicity, for example, by oxygen plasma, as discussed below.

Interlayer nanostructures of GO membranes, as shown in our previous study,<sup>30</sup> strongly depend on the fabrication

conditions; in the vacuum filtration deposition process, slow deposition rate leads to thermodynamically more stable interlayer nanostructure. In this work, in order to minimize the GO deposition rate and thus form few-layered GO membranes with thermodynamically more stable interlayer nanostructure, a slow layer-by-layer (LBL) deposition method was applied during vacuum filtration deposition. As shown in Figure 1, SLGO flakes were deposited by vacuum filtration in a layer-by-layer fashion; the second and the subsequent layers of GO were added as the previous layer(s) was deposited and completely dried under vacuum at room temperature. By this method, the previous GO layer(s) could significantly decrease the deposition rate of the next layer, allowing long time for GO flakes to assemble and form thermodynamically more stable interlayer nanostructure. Figure S3 indicates as GO deposition layer increased from one to two and three layers, pure water permeance decreased from 160.4 to 42.3 and 9.2 L/( $m^2 \cdot h \cdot bar$ ), respectively. After thermal reduction, water permeance of onelayered and double-layered rGO membranes significantly dropped to 37.8 and 9.5 L/(m<sup>2</sup>·h·bar); for the triple-layered rGO membrane, no water permeation under pressure drop of 5 bar (water permeance <1.0 L/(m<sup>2</sup>·h·bar)) was detected after 24 h. This suggests the triple-layered rGO membrane has high quality and probably only very small hydrophobic nanochannels exist, which need high breakthrough pressure before water can permeate through. 42,43,34 These water permeation results reveal that the hydrophobic nature and ~0.6 nm pores of rGO membranes might impede their direct application in water nanofiltration. However, if hydrophilic pores/nanochannels with size larger than water molecule but smaller than solute particles could be generated on rGO membranes through controllable surface modifications, such as plasma etching, UV-irradiation or ion bombardment, the high-quality triple-layered rGO membranes could show great potential for high flux and high selectivity water nanofiltration application.

Field emission scanning electron microscopy (FESEM) was employed to examine the surface morphology of the triplelayered rGO membrane. Compared with the bare AAO substrate (Figure S4), the ultrathin rGO coating is so thin that the substrate pores can still be clearly observed (Figure 2A), but all the pores of AAO substrate are well covered and no pin-holes can be found. Thickness of the triple-layered rGO membrane is about 5 nm, as determined from the crosssectional SEM image (Figure 2B).

In this study, oxygen plasma was employed to modify the surface properties of the triple-layered rGO membranes. Before applying oxygen plasma on the rGO membranes, influence of **Industrial & Engineering Chemistry Research** 

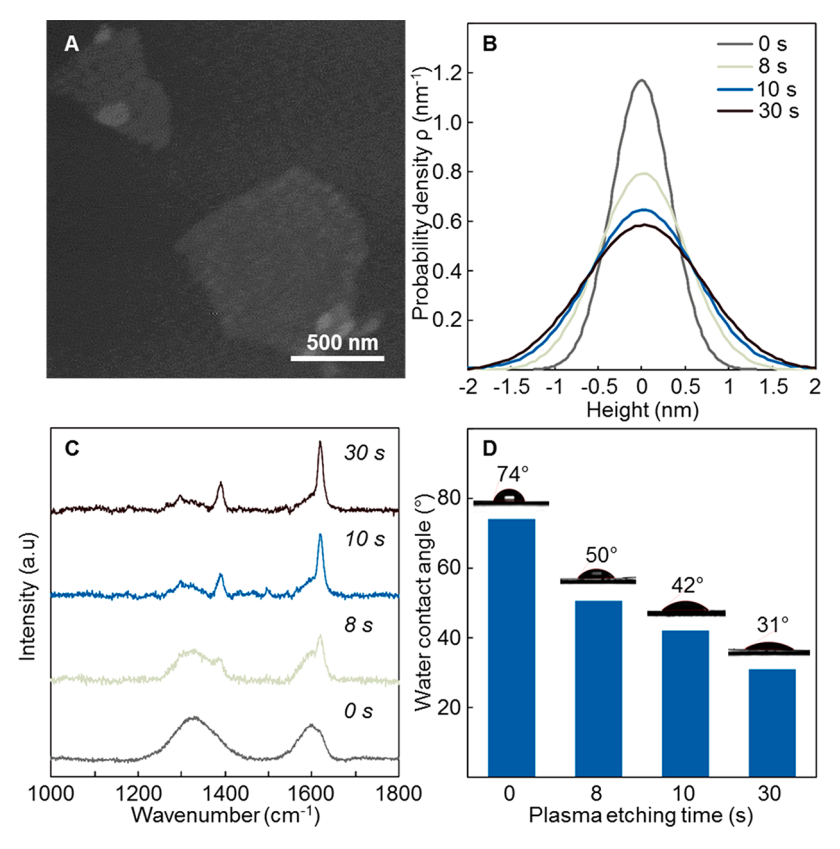


Figure 3. Characterization of single-layer rGO flakes and triple-layered rGO membranes exposed to different plasma treatment duration: (A) AFM images of rGO flakes exposed to oxygen plasma treatment for 8 s; (B) Height distributions of the rGO flakes exposed to plasma etching for different times. The solid line is the Gaussian fit of the height distribution. To clarify the roughness difference between rGO flakes treated with different plasma etching conditions, the mean of the Gaussian fit was set as zero and the height distribution curve was shifted accordingly as well; (C) Raman spectra of the rGO flakes exposed to plasma etching for different times; (D) Water contact angle of triple-layered rGO membranes etched under different oxygen plasma durations.

oxygen plasma treatment on individual rGO flakes was investigated. Figure S5A shows a representative AFM image of rGO flakes without plasma treatment; the single layer rGO flakes appear rather featureless and flat. Figure 3A,B illustrates the morphology and surface roughness change of rGO flakes after being exposed to plasma etching for different times. Compared with GO without plasma etching, 8-s treated rGO flakes (Figure 3A) showed no obvious morphology change except the appearance of some rounded pits. With the increase of plasma treatment time to 10 and 30 s, the pits tended to grow in number and expand, and eventually made the rGO flakes less visible (Figure S5B,C). Topological change of rGO flakes after different plasma etching times was also characterized by measuring surface roughness,<sup>44</sup> as shown in the height distribution diagram (Figure 3B). The Gaussian fit for the height distribution of the original rGO flake presents a full width at half-maximum (fwhm) of 0.77 nm; as plasma treatment applied, the fwhm extended to 1.18 nm for 8-s etched rGO flakes, 1.42 and 1.62 nm for 10- and 30-s etched rGO flakes, respectively, indicating the surface of rGO flakes became rougher and rougher with the increase of oxygen plasma exposure time. Apparently, the incremental increase of surface roughness is due to the progressively increased small defects created by the oxidation of rGO flakes.<sup>45</sup> Therefore, if appropriate oxygen plasma treatment was applied on the triplelayered rGO membranes, the nanopores with size larger than water molecule but smaller than solute particles might be

generated and thus enhance water permeation, while maintaining highly selective nanofiltration performance.

Raman, XPS and water contact angle measurements were employed to characterize the effects of oxygen plasma etching on the chemical modification and surface hydrophilicity of the triple-layered rGO membranes. Figure 3C shows the Raman spectra of rGO membranes treated with different oxygen plasma exposure times (0-30 s). We found a new CH<sub>2</sub> (or CH<sub>3</sub>) asymmetric vibration band located at ~1390 cm<sup>-1</sup> and a D' band at  $\sim 1622$  cm<sup>-1</sup> after 8 s of plasma treatment. With prolonged plasma etching duration of 10 and 30 s, the intensity of CH<sub>2</sub> (or CH<sub>3</sub>) and D' bands increased significantly, indicating the incremental sp<sup>3</sup> distortion of rGO flakes caused by the incorporation of oxygen-containing functional groups. 46,47 XPS measurements of oxygen plasma etched triple-layered rGO membranes were conducted to further clarify the influence of plasma etching on the elemental composition of the membranes (Figure S6). Upon plasma treatment, the C/O atomic ratio decreased with the increase of the etching duration (Table 1), and the relative amount of C— O bonded functional groups on triple-layered rGO membranes increased from 18.7% to 26.3%, suggesting more hydroxyl groups were created by plasma etching. XPS results listed in Table 1 further suggest that the oxidation degree and/or the relative amount of oxygen-containing functional groups of the rGO membranes may be tuned by the plasma treatment. Moreover, the XPS results are also consistent with the change of the surface hydrophilicity of the etched rGO membranes, as

Table 1. Relative Amount of C-O Bond and Carbon/ Oxygen Ratio of Triple-Layered rGO Membranes Exposed to Different Oxygen Plasma Etching Time

Etching Time (s)	С—О	C:O
0	18.7%	8.0:1
8	22.4%	4.8:1
10	23.6%	3.8:1
30	26.3%	3.0:1

shown in Figure 3D; because of the incrementally introduced hydrophilic hydroxyl groups, the water contact angle of the rGO membranes decreases as the etching time increases, indicating the rGO membrane surface hydrophilicity improves with oxygen plasma treatment. Therefore, by adjusting membrane pores and membrane hydrophilicity, oxygen plasma treatment on triple-layered rGO membranes with appropriate durations could significantly improve their nanofiltration performance.

Pure water permeation was conducted to study the transport characteristics of oxygen plasma etched, triple-layered rGO membranes. Water permeance of rGO membranes treated by different plasma exposure times was measured, and the results are shown in Figure 4A. After the triple-layered rGO membranes were exposed to 8–30 s oxygen plasma treatment, water permeance increased from <1.0 L/(m²·h·bar) of the nontreated rGO membrane to 4.3–43.7 L/(m²·h·bar). However, with more than 2 min plasma exposure, the rGO layer of the membrane could be fully etched away so that water permeance of the corresponding membranes was close to that of the bare AAO substrate. Therefore, to avoid overetching of rGO layers, we kept the plasma treatment duration less than 2 min.

Water nanofiltration performance of plasma etched, triple-layered rGO membranes was examined by measuring the rejection for methylene blue (MB) (cationic dye; MW: 373.90 g·mol<sup>-1</sup>; molecular dimension: 0.7 nm × 1.6 nm). As shown in Figure 4B, the 8-s etched rGO membrane exhibits a high rejection (98%) for MB after 2 h of filtration. Upon 10 s of plasma treatment, similar MB rejection (97%) was observed for the corresponding rGO membrane. After 30 s of oxygen plasma exposure, the dye rejection slightly declined to approximately 90%. However, the MB rejection dropped drastically to 50% after 60 s plasma exposure, apparently because the rGO membrane was overetched and thus large,

nonselective defects were generated. Applying appropriate oxygen plasma treatment on the triple-layered rGO membranes, therefore, drastically increases water permeance while maintaining high rejection for MB, resulting from the improved hydrophilicity and introduction of more defects smaller than MB on rGO flakes for water transport. Oxygen plasma here has been shown as an effective technique to tune water nanofiltration performance by simply adjusting oxygen plasma treatment time.

## 4.0. CONCLUSION

In conclusion, oxygen plasma has been shown as an effective method to tune the water nanofiltration performance of fewlayered, water-tight rGO membranes. Upon oxygen plasma treatment, hydrophilicity of the rGO membranes was improved via decreasing C/O ratio and/or introducing more oxygen-containing functional groups, such as hydroxyl groups, and small structural defects on rGO flakes were introduced by oxidizing carbon from rGO flakes. As a synergistic combined effect, water nanofiltration performance for MB, as an example, was tuned by adjusting oxygen plasma treatment time; after 30 s of plasma etching, water permeance as high as  $43.7 \text{ L/(m}^2 \cdot \text{h} \cdot \text{m}^2 \cdot$ bar) and rejection for MB higher than 90% were obtained, whereas 10 s etching of led to water permeance of 6.0 L/( $m^2 \cdot h$ · bar) and MB rejection of 98%. Depending on the size and target rejection of the potential contaminants that need to be excluded in water nanofiltration, appropriate oxygen plasma etching time may be identified accordingly. Compared with single-layered graphene membranes that are very difficult to be fabricated in large scale and in high quality, few-layered rGO membranes can be facilely fabricated by solution-based deposition process and subsequent reduction. Moreover, oxygen plasma etching on few-layered rGO membranes, instead of single-layered graphene membranes, may allow better control over the etching process and avoid overetching. Few-layered rGO membranes, therefore, may be appropriately designed by adjusting oxygen plasma treatment conditions for various nanofiltration applications.

# ASSOCIATED CONTENT

#### **Supporting Information**

The Supporting Information is available free of charge on the ACS Publications website at DOI: 10.1021/acs.iecr.8b02206.

Characterizations of single layer GO prepared by freeze-thaw method, including AFM, Raman and

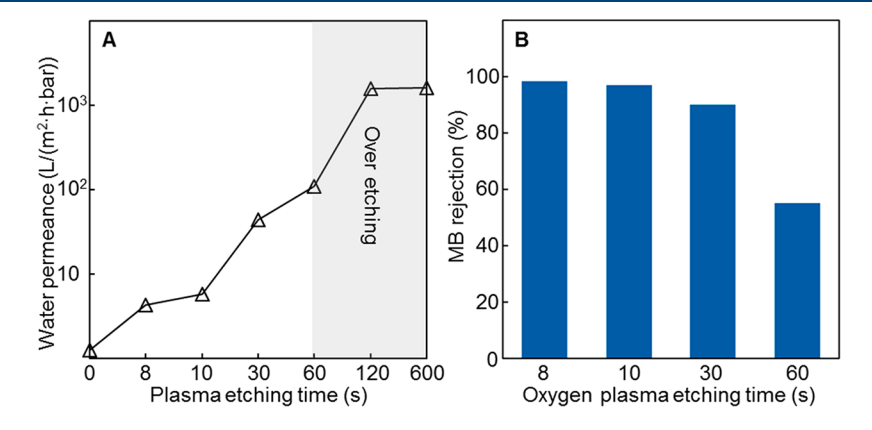


Figure 4. Permeation performance for the plasma etched triple-layered rGO membranes: (A) pure water permeation through rGO membranes exposed to different plasma etching time; (B) methylene blue (MB) rejection of rGO membranes exposed to different plasma treatment times.

FTIR; XPS spectrum of GO/rGO membranes and plasma etched triple-layered rGO membranes; XRD of dry/wet state GO and rGO membranes; water permeance of GO/rGO membranes with different layers of GO deposition; SEM image of AAO substrate; AFM topological scan of rGO flakes with different time of plasma etching (PDF)

## AUTHOR INFORMATION

#### **Corresponding Author**

\*M. Yu. E-mail: yum5@rpi.edu.

ORCID ®

Miao Yu: 0000-0003-4730-7563

Notes

The authors declare no competing financial interest.

# ACKNOWLEDGMENTS

We gratefully acknowledge the support by National Science Foundation (NSF) Career Award under Grant No. 1451887.

### ABBREVIATIONS

AFM = atomic force microscopy

FTIR = Fourier transform infrared

SEM = scanning electron microscopy

SLGO = single-layer graphene oxide

rGO = reduced graphene oxide

XPS = X-ray photoelectron spectroscopy

XRD = X-ray diffraction

## REFERENCES

- (1) Vorosmarty, C. J.; McIntyre, P. B.; Gessner, M. O.; Dudgeon, D.; Prusevich, A.; Green, P.; Glidden, S.; Bunn, S. E.; Sullivan, C. A.; Liermann, C. R.; Davies, P. M. Global threats to human water security and river biodiversity (vol 467, pg 555, 2010). *Nature* **2010**, 468 (7321), 334–334.
- (2) Shannon, M. A.; Bohn, P. W.; Elimelech, M.; Georgiadis, J. G.; Marinas, B. J.; Mayes, A. M. Science and technology for water purification in the coming decades. *Nature* **2008**, *452* (7185), 301–310.
- (3) Elimelech, M. The global challenge for adequate and safe water. *Aqua* **2006**, *S5* (1), 3–10.
- (4) Fu, F. L.; Wang, Q. Removal of heavy metal ions from wastewaters: A review. J. Environ. Manage. 2011, 92 (3), 407–418.
- (5) Chakraborti, D.; Rahman, M. M.; Das, B.; Murrill, M.; Dey, S.; Mukherjee, S. C.; Dhar, R. K.; Biswas, B. K.; Chowdhury, U. K.; Roy, S.; Sorif, S.; Selim, M.; Rahman, M.; Quamruzzaman, Q. Status of groundwater arsenic contamination in Bangladesh: A 14-year study report. *Water Res.* **2010**, *44* (19), 5789–5802.
- (6) Kimura, K.; Toshima, S.; Amy, G.; Watanabe, Y. Rejection of neutral endocrine disrupting compounds (EDCs) and pharmaceutical active compounds (PhACs) by RO membranes. *J. Membr. Sci.* **2004**, 245 (1–2), 71–78.
- (7) Comerton, A. M.; Andrews, R. C.; Bagley, D. M.; Hao, C. Y. The rejection of endocrine disrupting and pharmaceutically active compounds by NF and RO membranes as a function of compound a water matrix properties. *J. Membr. Sci.* **2008**, *313* (1–2), 323–335.
- (8) Basile, T.; Petrella, A.; Petrella, M.; Boghetich, G.; Petruzzelli, V.; Colasuonno, S.; Petruzzelli, D. Review of Endocrine-Disrupting-Compound Removal Technologies in Water and Wastewater Treatment Plants: An EU Perspective. *Ind. Eng. Chem. Res.* **2011**, 50 (14), 8389–8401.
- (9) Song, Z. N.; Fathizadeh, M.; Huang, Y.; Chu, K. H.; Yoon, Y. M.; Wang, L.; Xu, W. W. L.; Yu, M. TiO2 nanofiltration membranes prepared by molecular layer deposition for water purification. *J. Membr. Sci.* **2016**, *510*, 72–78.

- (10) Dikin, D. A.; Stankovich, S.; Zimney, E. J.; Piner, R. D.; Dommett, G. H. B.; Evmenenko, G.; Nguyen, S. T.; Ruoff, R. S. Preparation and characterization of graphene oxide paper. *Nature* **2007**, *448* (7152), 457–460.
- (11) Lee, C.; Wei, X. D.; Kysar, J. W.; Hone, J. Measurement of the elastic properties and intrinsic strength of monolayer graphene. *Science* **2008**, *321* (5887), 385–388.
- (12) Geim, A. K.; Novoselov, K. S. The rise of graphene. *Nat. Mater.* **2007**, *6* (3), 183–191.
- (13) Geim, A. K. Graphene: Status and Prospects. Science 2009, 324 (5934), 1530-1534.
- (14) Dreyer, D. R.; Park, S.; Bielawski, C. W.; Ruoff, R. S. The chemistry of graphene oxide. *Chem. Soc. Rev.* **2010**, 39 (1), 228–240.
- (15) Fathizadeh, M.; Xu, W. W. L.; Zhou, F. L.; Yoon, Y.; Yu, M. Graphene Oxide: A Novel 2-Dimensional Material in Membrane Separation for Water Purification. *Adv. Mater. Interfaces* **2017**, *4* (5), 1600012
- (16) Zhou, F. L.; Tien, H. N.; Xu, W. W. L.; Chen, J. T.; Liu, Q. L.; Hicks, E.; Fathizadeh, M.; Li, S. G.; Yu, M. Ultrathin graphene oxide-based hollow fiber membranes with brush-like CO<sub>2</sub>-philic agent for highly efficient CO<sub>2</sub> capture. *Nat. Commun.* **2017**, 8, DOI: 10.1038/s41467-017-02318-1.
- (17) Qin, Y. Z.; Hu, Y. Y.; Koehler, S.; Cai, L. H.; Wen, J. J.; Tan, X. J.; Xu, W. W. L.; Sheng, Q.; Hou, X.; Xue, J. M.; Yu, M.; Weitz, D. Ultrafast Nanofiltration through Large-Area Single-Layered Graphene Membranes. ACS Appl. Mater. Interfaces 2017, 9 (11), 9239—9244.
- (18) Konatham, D.; Yu, J.; Ho, T. A.; Striolo, A. Simulation Insights for Graphene-Based Water Desalination Membranes. *Langmuir* **2013**, 29 (38), 11884–11897.
- (19) Lin, L. C.; Grossman, J. C. Atomistic understandings of reduced graphene oxide as an ultrathin-film nanoporous membrane for separations. *Nat. Commun.* **2015**, *6*, DOI: 10.1038/ncomms9335.
- (20) Wang, Y. H.; He, Z. J.; Gupta, K. M.; Shi, Q.; Lu, R. F. Molecular dynamics study on water desalination through functionalized nanoporous graphene. *Carbon* **2017**, *116*, 120–127.
- (21) Jain, T.; Rasera, B. C.; Guerrero, R. J. S.; Boutilier, M. S. H.; O'Hern, S. C.; Idrobo, J. C.; Karnik, R. Heterogeneous subcontinuum ionic transport in statistically isolated graphene nanopores. *Nat. Nanotechnol.* **2015**, *10* (12), 1053.
- (22) Rollings, R. C.; Kuan, A. T.; Golovchenko, J. A. Ion selectivity of graphene nanopores. *Nat. Commun.* **2016**, *7*, 11408.
- (23) O'Hern, S. C.; Stewart, C. A.; Boutilier, M. S. H.; Idrobo, J. C.; Bhaviripudi, S.; Das, S. K.; Kong, J.; Laoui, T.; Atieh, M.; Karnik, R. Selective Molecular Transport through Intrinsic Defects in a Single Layer of CVD Graphene. ACS Nano 2012, 6 (11), 10130–10138.
- (24) O'Hern, S. C.; Boutilier, M. S. H.; Idrobo, J. C.; Song, Y.; Kong, J.; Laoui, T.; Atieh, M.; Karnik, R. Selective Ionic Transport through Tunable Subnanometer Pores in Single-Layer Graphene Membranes. *Nano Lett.* **2014**, *14* (3), 1234–1241.
- (25) Kidambi, P. R.; Boutilier, M. S. H.; Wang, L. D.; Jang, D.; Kim, J.; Karnik, R. Selective Nanoscale Mass Transport across Atomically Thin Single Crystalline Graphene Membranes. *Adv. Mater.* **2017**, *29* (19), 1605896.
- (26) Surwade, S. P.; Smirnov, S. N.; Vlassiouk, I. V.; Unocic, R. R.; Veith, G. M.; Dai, S.; Mahurin, S. M. Water desalination using nanoporous single-layer graphene (vol 10, pg 459, 2015). *Nat. Nanotechnol.* **2016**, *11* (11), 995–995.
- (27) Thiele, C.; Felten, A.; Echtermeyer, T. J.; Ferrari, A. C.; Casiraghi, C.; von Lohneysen, H.; Krupke, R. Electron-beam-induced direct etching of graphene. *Carbon* **2013**, *64*, 84–91.
- (28) Liu, L.; Xie, D. L.; Wu, M. H.; Yang, X. X.; Xu, Z.; Wang, W. L.; Bai, X. D.; Wang, E. G. Controlled oxidative functionalization of monolayer graphene by water-vapor plasma etching. *Carbon* **2012**, *50* (8), 3039–3044.
- (29) Li, H.; Huang, Y.; Mao, Y. T.; Xu, W. W. L.; Ploehn, H. J.; Yu, M. Tuning the underwater oleophobicity of graphene oxide coatings via UV irradiation. *Chem. Commun.* **2014**, *50* (69), 9849–9851.
- (30) Xu, W. W. L.; Fang, C.; Zhou, F. L.; Song, Z. N.; Liu, Q. L.; Qiao, R.; Yu, M. Self-Assembly: A Facile Way of Forming Ultrathin,

- High-Performance Graphene Oxide Membranes for Water Purification. *Nano Lett.* **2017**, *17* (5), 2928–2933.
- (31) Han, Y.; Xu, Z.; Gao, C. Ultrathin Graphene Nanofiltration Membrane for Water Purification. *Adv. Funct. Mater.* **2013**, 23 (29), 3693–3700.
- (32) Liang, B.; Zhang, P.; Wang, J. Q.; Qu, J.; Wang, L. F.; Wang, X. X.; Guan, C. F.; Pan, K. Membranes with selective laminar nanochannels of modified reduced graphene oxide for water purification. *Carbon* **2016**, *103*, 94–100.
- (33) Chen, X. F.; Qiu, M. H.; Ding, H.; Fu, K. Y.; Fan, Y. Q. A reduced graphene oxide nanofiltration membrane intercalated by well-dispersed carbon nanotubes for drinking water purification. *Nanoscale* **2016**, *8* (10), 5696–5705.
- (34) Huang, L.; Chen, J.; Gao, T. T.; Zhang, M.; Li, Y. R.; Dai, L. M.; Qu, L. T.; Shi, G. Q. Reduced Graphene Oxide Membranes for Ultrafast Organic Solvent Nanofi Itration. *Adv. Mater.* **2016**, *28* (39), 8669–8674.
- (35) Harpale, A.; Chew, H. B. Hydrogen-plasma patterning of multilayer graphene: Mechanisms and modeling. *Carbon* **2017**, *117*, 82–91.
- (36) Marcano, D. C.; Kosynkin, D. V.; Berlin, J. M.; Sinitskii, A.; Sun, Z. Z.; Slesarev, A.; Alemany, L. B.; Lu, W.; Tour, J. M. Improved Synthesis of Graphene Oxide. *ACS Nano* **2010**, *4* (8), 4806–4814.
- (37) Ogino, I.; Yokoyama, Y.; Iwamura, S.; Mukai, S. R. Exfoliation of Graphite Oxide in Water without Sonication: Bridging Length Scales from Nanosheets to Macroscopic Materials. *Chem. Mater.* **2014**, *26* (10), 3334–3339.
- (38) Ferrari, A. C.; Robertson, J. Interpretation of Raman spectra of disordered and amorphous carbon. *Phys. Rev. B: Condens. Matter Mater. Phys.* **2000**, 61 (20), 14095–14107.
- (39) Graf, D.; Molitor, F.; Ensslin, K.; Stampfer, C.; Jungen, A.; Hierold, C.; Wirtz, L. Spatially resolved raman spectroscopy of single-and few-layer graphene. *Nano Lett.* **2007**, 7 (2), 238–242.
- (40) Joshi, R. K.; Carbone, P.; Wang, F. C.; Kravets, V. G.; Su, Y.; Grigorieva, I. V.; Wu, H. A.; Geim, A. K.; Nair, R. R. Precise and Ultrafast Molecular Sieving Through Graphene Oxide Membranes. *Science* **2014**, 343 (6172), 752–754.
- (41) Zheng, S. X.; Tu, Q. S.; Urban, J. J.; Li, S. F.; Mi, B. X. Swelling of Graphene Oxide Membranes in Aqueous Solution: Characterization of Interlayer Spacing and Insight into Water Transport Mechanisms. ACS Nano 2017, 11 (6), 6440–6450.
- (42) Su, Y.; Kravets, V. G.; Wong, S. L.; Waters, J.; Geim, A. K.; Nair, R. R. Impermeable barrier films and protective coatings based on reduced graphene oxide. *Nat. Commun.* **2014**, *5*, DOI: 10.1038/ncomms5843.
- (43) Liu, H. Y.; Wang, H. T.; Zhang, X. W. Facile Fabrication of Freestanding Ultrathin Reduced Graphene Oxide Membranes for Water Purification. *Adv. Mater.* **2015**, 27 (2), 249–254.
- (44) Rezania, B.; Severin, N.; Talyzin, A. V.; Rabe, J. P. Hydration of Bilayered Graphene Oxide. *Nano Lett.* **2014**, *14* (7), 3993–3998.
- (45) Solis-Fernandez, P.; Paredes, J. I.; Villar-Rodil, S.; Guardia, L.; Fernandez-Merino, M. J.; Dobrik, G.; Biro, L. P.; Martinez-Alonso, A.; Tascon, J. M. D. Global and Local Oxidation Behavior of Reduced Graphene Oxide. *J. Phys. Chem. C* 2011, 115 (16), 7956–7966.
- (46) Dresselhaus, M. S.; Jorio, A.; Souza Filho, A. G.; Saito, R. Defect characterization in graphene and carbon nanotubes using Raman spectroscopy. *Philos. Trans. R. Soc., A* **2010**, 368 (1932), 5355–5377.
- (47) Yang, R.; Shi, Z. W.; Zhang, L. C.; Shi, D. X.; Zhang, G. Y. Observation of Raman G-Peak Split for Graphene Nanoribbons with Hydrogen-Terminated Zigzag Edges. *Nano Lett.* **2011**, *11* (10), 4083–4088.